

Local spin structure in the layered van der Waals materials $\text{MnPS}_x\text{Se}_{3-x}$

Raju Baral,^{1,*} Amanda V. Haglund,² Jue Liu,¹ Alexander I. Kolesnikov,¹ David Mandrus,^{2,3} and Stuart Calder^{1,†}

¹*Neutron Scattering Division, Oak Ridge National Laboratory, Oak Ridge, Tennessee 37831, USA.*

²*Department of Materials Science and Engineering,
University of Tennessee, Knoxville, TN 37996, USA.*

³*Materials Science and Technology Division, Oak Ridge National Laboratory, Oak Ridge, TN 37831, USA.*

Two-dimensional (2D) layered materials, whether in bulk form or reduced to just a single layer, have potential applications in spintronics and capacity for advanced quantum phenomena. A prerequisite for harnessing these opportunities lies in gaining a comprehensive understanding of the spin behavior in 2D materials. The low dimensionality motivates an understanding of the spin correlations over a wide length scale, from local to long range order. In this context, we focus on the magnetism in bulk MnPSe_3 and MnPS_3 , 2D layered van der Waals antiferromagnetic semiconductors. These materials have similar honeycomb Mn layers and magnetic ordering temperatures, but distinct spin orientations and exchange interactions. We utilize neutron scattering to gain deeper insights into the local magnetic structures and spin correlations in the paramagnetic and ordered phases by systematically investigating a $\text{MnPS}_x\text{Se}_{3-x}$ ($x = 0, 1, 1.5, 2, 3$) series of powder samples using total neutron scattering measurements. By employing magnetic pair distribution function (mPDF) analysis, we unraveled the short-range magnetic correlations in these materials and explored how the non-magnetic anion S/Se mixing impacts the magnetic correlations. The results reveal that the magnetism can be gradually tuned through alteration of the non-magnetic S/Se content, which tunes the atomic structure. The change in magnetic structure is also accompanied by a control of the magnetic correlation length within the 2D honeycomb layers. Complimentary inelastic neutron scattering measurements allowed a quantification of the change in the magnetic exchange interactions for the series and further highlighted the gradual evolution of spin interactions in the series $\text{MnPS}_x\text{Se}_{3-x}$.

I. INTRODUCTION

Reducing the dimensionality of a compound down to topologically constrained layers can uncover new and intriguing behaviors that go beyond well-established classical understanding. A prime example is graphene, in which a single layer is extracted from the weakly connected van der Waals (VDW) bonded layers in graphite [1]. Graphene and other 2D materials have undergone significant interest stemming from their potential to exhibit novel quantum effects, such as Dirac semi-metal and quantum anomalous Hall insulating behavior [2, 3]. Interesting properties can be found in materials ranging from the ideal two-dimensional (2D) monolayers to quasi-2D materials with more complex bulk VDW-bonded structures [4]. Developing functional spintronic materials typically relies on harnessing magnetic and semiconducting properties, however, graphene lacks these phenomena. As a result, 2D VDW materials that have intrinsic magnetism and semiconductivity with a honeycomb arrangement are of interest. A prerequisite for developing functional magnetic materials and uncovering novel quantum behavior in 2D materials lies in gaining a comprehensive understanding of the spin behavior over the relevant length scales.

MnPS_3 and MnPSe_3 are layered VDW antiferromagnetic materials that possess both magnetic and semi-

conducting properties, with the magnetic ions adopting the same hexagonal motif as graphene. Although each crystallizes in different space groups, MnPS_3 in $C2/m$ and MnPSe_3 in $R\bar{3}$, they have nearly identical Néel temperatures of 78 K for MnPS_3 and 74 K for MnPSe_3 [5, 6]. Both of these compositions contain an equivalent fraction of magnetic ions ($n_s = 1/5$) within their unit cells and are $S = 5/2$ materials. Despite their similar transition temperatures and magnetic ion content, intriguing distinctions become apparent in their magnetic behavior. MnPS_3 has Heisenberg antiferromagnetic spins that point out of the hexagonal ab -plane [7], while MnPSe_3 displays XY anisotropy in its magnetic behavior with spins lying in the ab -plane [8]. The crystal structures with spin directions are shown in Fig. 1.

By altering the non-magnetic S and Se ion content it is possible to chemically tune between MnPS_3 and MnPSe_3 in the series $\text{MnPS}_x\text{Se}_{3-x}$. This provides a way to explore and understand the evolution between the two magnetic states. Stabilization of this series has been shown for a wide concentration of x values for powders and single crystal samples [9–12]. Based on bulk characterizations, these studies have found indications of a change in the magnetic ordering within the series as x is altered. This motivates further investigation to probe the microscopic spin states and magnetic exchange interactions.

In this work, we present total neutron scattering and inelastic neutron scattering measurements to achieve a comprehensive picture of the long-range and short-range correlations and exchange interactions in the series $\text{MnPS}_x\text{Se}_{3-x}$ ($x = 0, 1, 1.5, 2, 3$). Using magnetic pair

* baralr@ornl.gov; lead contact

† caldersa@ornl.gov

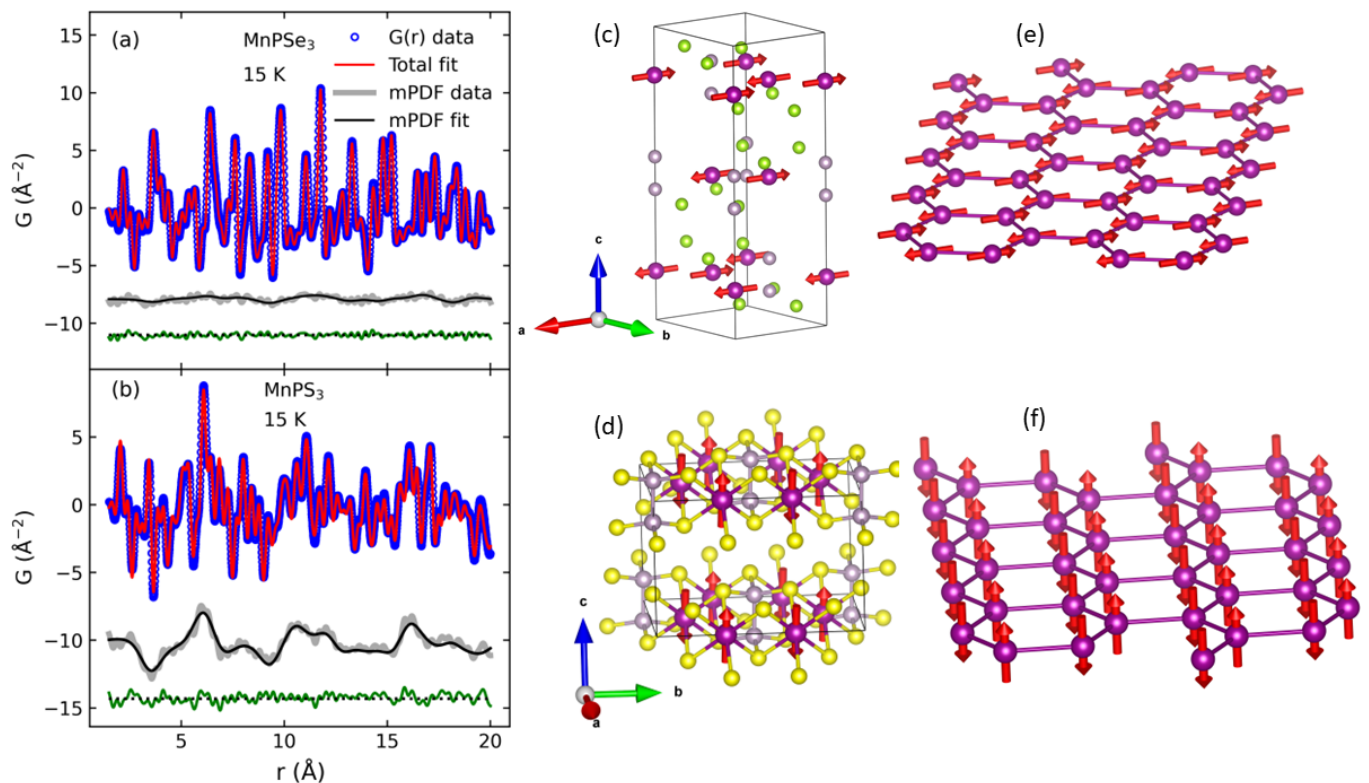


FIG. 1. The total neutron PDF (including both magnetic and nuclear scattering) and isolated magnetic PDF of (a) MnPSe_3 and (b) MnPS_3 at 15 K. The blue symbols and red curve represent the experimental total PDF data and total PDF fit, respectively. The gray and black curves represent the isolated magnetic PDF data and magnetic PDF fit (vertically offset for clarity). The green curve represents the overall fit residual. (c) Crystal structure of MnPSe_3 with Mn spins pointing in ab -plane (space group= $R\bar{3}$). (d) Crystal structure of MnPS_3 with Mn spins pointing out of the ab -plane (space group= $C2/m$). The hexagonal motif of the Mn ions for (e) MnPSe_3 and (f) MnPS_3 . Purple, gray, green, and yellow spheres represent the Mn, P, Se, and S atoms respectively.

distribution function (mPDF) analysis of total neutron scattering data, we present the real-space visualization of local spin-spin correlations in the paramagnetic state. The neutron scattering data reveals signatures of short-range magnetic correlations well above the Néel temperature for MnPS_3 and we modeled this with mPDF analysis to extract the short- and long-range spin states. As the S content increases towards MnPSe_3 the quasi-2D behavior is reduced, as shown by the decrease in the magnetic correlation length. This behavior is confirmed by inelastic neutron scattering measurements that show an increase in the interlayer exchange interactions as the Se content increases. We show that control of the non-magnetic S and Se content provides a sensitive mechanism to tune the magnetic spin direction between in-plane and out-of-plane through alteration of the crystal structure and small modifications in the Mn-Mn distances. This suggests routes beyond chemical pressure, such as strain, could provide promising routes to tune the magnetism in layered materials. Moreover the methodology employed of mPDF, that can access various spin length scales over a wide temperature range, is shown to be well suited to 2D VDW materials that can intrinsically contain com-

peting dimensionality of spin ordering.

II. EXPERIMENTAL METHODS

A. Sample synthesis

Polycrystalline samples of MnPSe_3 and MnPS_3 were synthesized following the standard solid-state reaction method as described in Ref. [8]. The samples MnPSSe_2 , $\text{MnPS}_{1.5}\text{Se}_{1.5}$, and MnPS_2Se were similarly synthesized using the identical method with suitable precursor materials. Confirmation of sample quality was accomplished through laboratory X-ray diffraction analysis.

B. Neutron total scattering

Neutron total scattering experiments were conducted on both the Nano Scale-Ordered Material Diffractometer (NOMAD) and the HB-2A powder diffractometer. NOMAD is a dedicated total scattering instrument for

PDF analysis. The HB-2A powder diffraction instrument is traditionally utilized for reciprocal space analysis at low Q , however here we use a short wavelength to access higher Q and perform total scattering measurements and PDF analysis. With the capabilities to measure samples at millikelvin temperatures and apply magnetic fields HB-2A can provide unique conditions for magnetic PDF analysis for a broad range of quantum material research.

For both the HB-2A and NOMAD data the atomic PDF fits were performed using PDFgui [13] and the magnetic PDF fits were obtained using diffpy.mpdf [14], a Python package designed for magnetic PDF calculations and fitting.

1. NOMAD

Measurements on MnPSe_3 and MnPS_3 were conducted at NOMAD, located at the Spallation Neutron Source (SNS), Oak Ridge National Laboratory (ORNL) [15]. These polycrystalline samples (MnPSe_3 and MnPS_3) were loaded into 6 mm vanadium cans in a helium glove box. Total scattering patterns were collected in a helium cryostat over a range of temperatures from 15 K to 300 K. The collected data was reduced and Fourier transformed with a Q_{max} value of 20 \AA^{-1} , employing automatic data reduction scripts at NOMAD [16]. The choice of Q_{max} value is critical. A high Q_{max} value can significantly improve the resolution in real space, but it also introduces statistical noise and artifacts. Consequently, a Q_{max} value of 20 \AA^{-1} was strategically selected to optimize the balance between achieving high resolution and minimizing noise artifacts.

2. HB-2A

Neutron total scattering patterns of the doped samples (MnPSSe_2 , $\text{MnPS}_{1.5}\text{Se}_{1.5}$, and MnPS_2Se) were collected on the HB-2A powder diffractometer at the High Flux Isotope Reactor (HFIR) at ORNL [17]. A vertically focusing germanium monochromator was used to select the wavelength of 1.12 \AA from the Ge(117) reflection. Approximately 5 grams of each sample were loaded into a vanadium sample holder inside a helium glove box. The total neutron scattering data for the doped samples were collected at temperatures of 15, 70, 125 and 300 K, with a collection time of four hours for each temperature point. The collected data were normalized using a vanadium standard measurement. The detector position and the wavelength of the neutron beam were calibrated with a Si measurement. Since HB-2A does not typically serve as a total scattering instrument, we processed the data further by performing a Fourier-transform using PDFgetN3 [18] with a Q_{max} value of 10 \AA^{-1} to produce the PDF data.

C. Inelastic neutron scattering

Inelastic neutron scattering (INS) measurements were conducted on MnPSSe_2 , $\text{MnPS}_{1.5}\text{Se}_{1.5}$, and MnPS_2Se using the Time-of-Flight Direct Geometry Spectrometer Sequoia [19] at the SNS, ORNL. An identical set-up was used compared to previous measurements on MnPSe_3 and MnPS_3 [8]. The samples were loaded into a cylindrical aluminum can with a diameter of 1 cm and INS spectra were measured using the three-sample changer within a closed-cycle refrigerator. Data were collected at incident energies of $E_i = 20 \text{ meV}$ and $E_i = 8 \text{ meV}$, both in high-resolution mode. For $E_i = 20 \text{ meV}$, the Fermi chopper operated at a frequency of 240 Hz, with a T_0 chopper frequency of 60 Hz, resulting in an energy resolution of 0.48 meV at the elastic line. Similarly, for $E_i = 8 \text{ meV}$, the Fermi chopper frequency was 120 Hz, and the T_0 chopper operated at 30 Hz, providing an energy resolution of 0.18 meV at the elastic line. The energy resolution was determined through DGS resolution, confirmed by analyzing cuts of the elastic line within the data. Momentum resolution (Q) was derived by fitting the resolution of the Bragg peaks at the elastic line. Measurements were taken over six hours at temperatures of 200 K, 100 K, 70 K, and 15 K.

The collected neutron data underwent reduction using Mantid [20]. The data were adjusted for the Bose thermal population factor. Initial data reduction and viewing were carried out using the DAVE software [21]. Modeling of the data was performed using SpinW [22].

III. RESULTS AND DISCUSSION

A. Atomic and magnetic PDF analysis of MnPSe_3 and MnPS_3

We begin with neutron total scattering measurements on MnPSe_3 and MnPS_3 , with a focus on probing the spin ordering over a wide temperature range through the magnetic ordering transitions. This is achieved through atomic and magnetic PDF analysis of the neutron scattering data, which allows for the same analysis methodology to be applied in both the long range ordered phase and short range paramagnetic phase. Fig. 1(a)-(b) shows the results at 15 K for MnPSe_3 and MnPS_3 . The total scattering data include both atomic and magnetic scattering, which need to be disentangled. To isolate the magnetic data we employed an iterative fitting approach. Initially, we used the known atomic structure to perform the atomic PDF fit [8]. Then, we subtracted the calculated atomic PDF from the total PDF data to obtain the residual. This residual contains a magnetic signal which was used for the initial magnetic PDF refinement. Following this, we refined the atomic PDF again, but this time using the total PDF data minus the best-fit magnetic PDF signal for the atomic PDF input. The refined parameters in the first iteration served as starting points

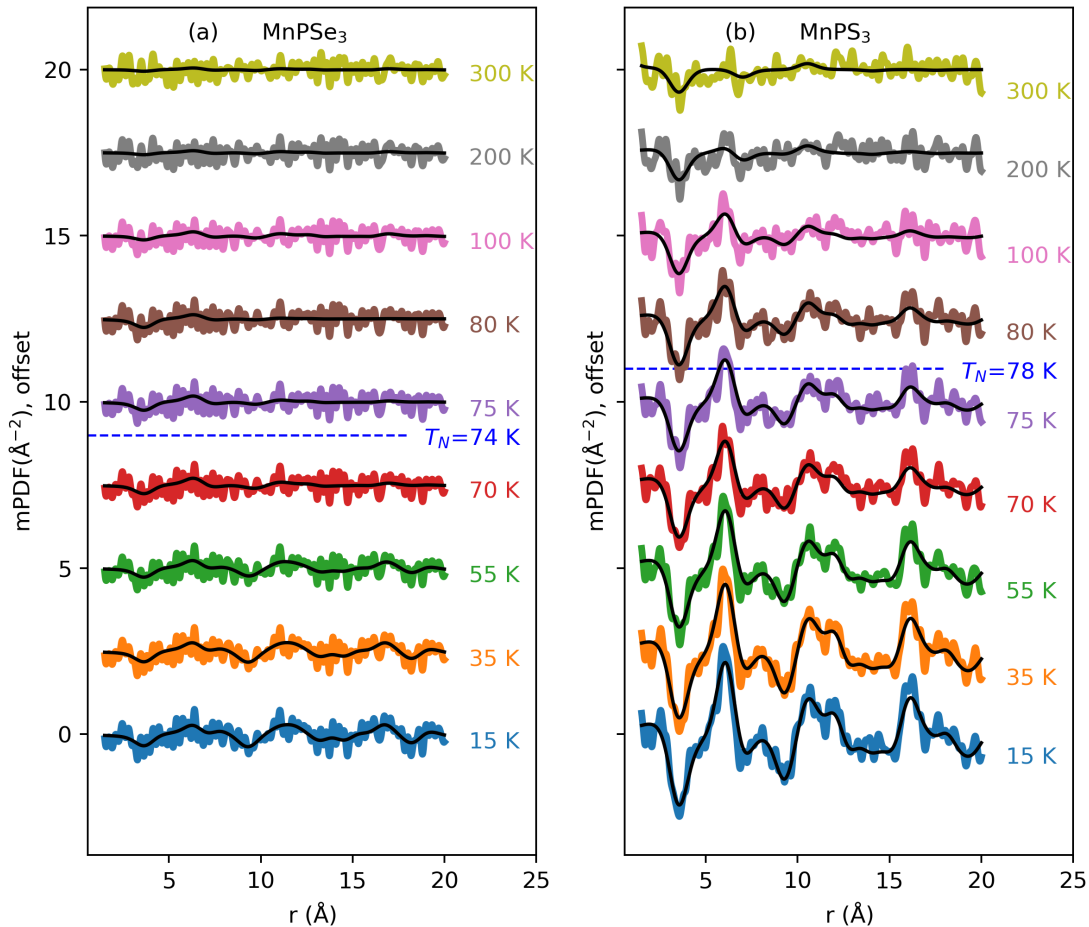


FIG. 2. Temperature series of the isolated magnetic PDF data and fits for MnPSe_3 (left) and MnPS_3 (right). The colored curves are the magnetic PDF data and the black curve represents the magnetic PDF fit (vertically offset for clarity). The long-range ordering transition temperature (T_N) is shown by the blue horizontal dashed line.

for the second iteration. We repeated this process for a third iteration, starting with the total PDF data minus the best-fit atomic PDF pattern from the second iteration, using the refined parameters from the second iteration. Finally, a third magnetic PDF fit was conducted. The detailed procedure of the iterative fitting approach of atomic and magnetic PDF is further discussed in the Supplementary section of Ref.[23].

The analysis was performed on a temperature grid ranging from 15 K to 300 K and the atomic and magnetic PDF patterns were calculated over a real space fitting range of 1.5 - 20 Å. For MnPSe_3 the low goodness of fit, $R_w = 0.0742$, is evident from the small, featureless fit residual illustrated by the green curve at the bottom of the panel. When allowed to freely refine, the lowest R_w occurs when the spins are at an angle of 70° with the c -axis, however using the previously reported value of 90° , where the spins are fixed to the ab -plane, produces a nearly identical fit [8]. Fig. 1(b) shows the atomic and magnetic PDF results for MnPS_3 , with $R_w = 0.139$. The optimal magnetic fit occurs when the spins are aligned

at an angle of $14.17 \pm 2.09^\circ$ with c -axis, which is comparable to previous studies [7].

We performed a series of atomic and magnetic PDF fits for various temperatures ranging from 15 to 300 K for both compositions. Fig. 2 shows the temperature series of the magnetic PDF fits for MnPSe_3 and MnPS_3 . For MnPSe_3 short range magnetic order persists above the Néel temperature ($T_N = 74$ K), up to 100 K and then decreases significantly beyond 100 K becoming almost unobservable at 200 K. Conversely in the case of MnPS_3 , we observed a strong magnetic PDF signal well above the Néel temperature ($T_N = 78$ K), with this local order magnetic signal persisting up to 300 K, which is the maximum temperature that the data were collected.

The mPDF analysis allows for a quantitative extraction of the magnetic correlation length and the ordered moment over a defined real space range. The ordered moment in the fitting range 1.5 - 20 Å as a function of temperature for MnPSe_3 and MnPS_3 are shown in Fig. 3(a). In the long range ordered regime the ordered moment begins to decrease exponentially as the sample

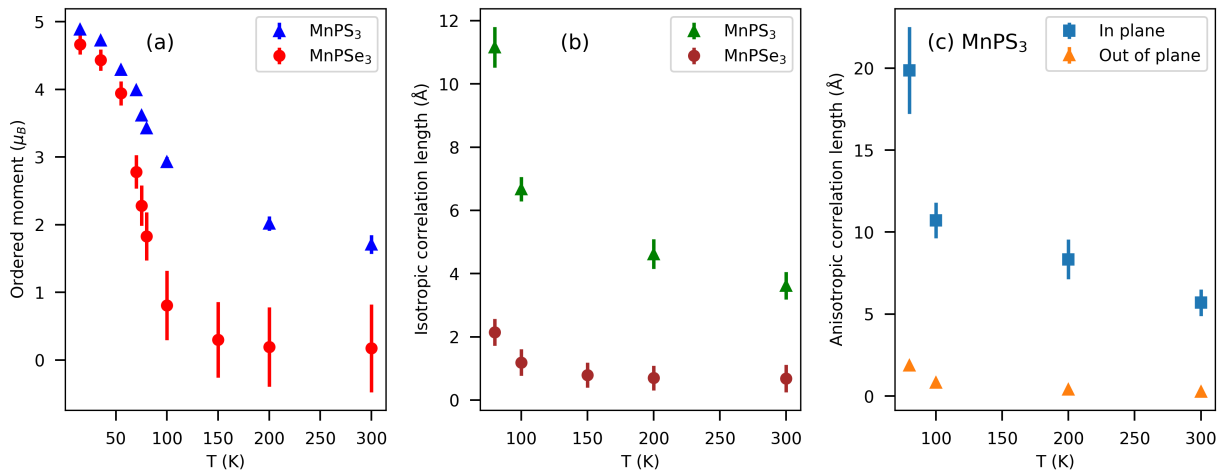


FIG. 3. (a) Magnetic moments as a function of temperature for MnPSe₃ and MnPS₃, evaluated within a fitting range from 1.5 to 20 Å. The red and blue symbols represent the ordered moment for MnPSe₃ and MnPS₃, respectively. (b) Variation of the correlation length with temperature in the paramagnetic regime for MnPSe₃ and MnPS₃, based on isotropic fits in the range of 1.5 to 20 Å. (c) Best fit correlation lengths in the *ab*-plane (blue squares) and along the *c*-axis (orange triangles) as a function of temperature in a paramagnetic regime for MnPS₃ using an anisotropic model. The error bars denote the standard deviation of the best-fit parameter values.

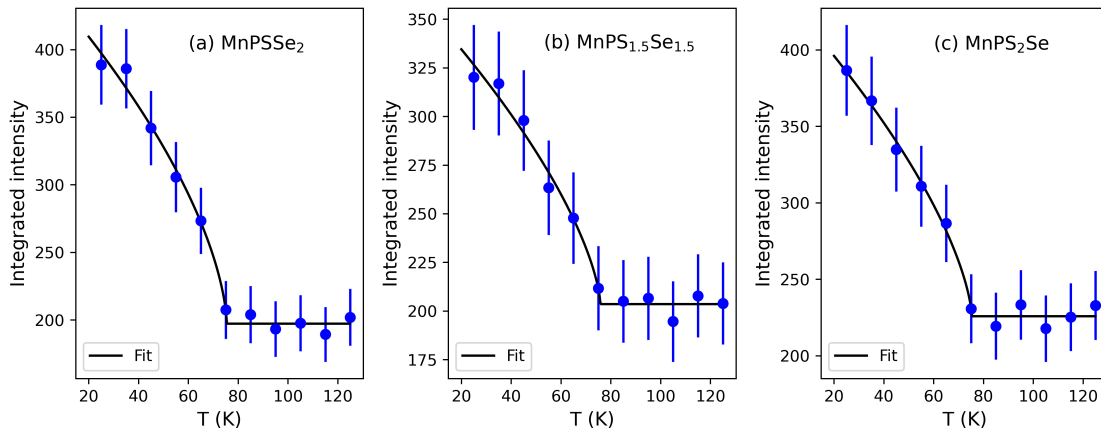


FIG. 4. Power law fit to the integrated intensity of a magnetic Bragg peak in the range $Q = 2.68$ to 2.73 Å⁻¹ for (a) MnPS₂Se₂, (b) MnPS_{1.5}Se_{1.5} and (c) MnPS₂Se.

temperature is increased towards the Néel temperature in both cases. With a further increase in temperature above the Néel temperature, the ordered moment further decreases. For MnPSe₃ the ordered moment approaches zero for temperatures of 150 K and above. For MnPS₃, however, while the ordered moment also decreases above the Néel temperature it attains a substantial moment of $1.7\mu_B$ at 300 K, 1/3 of the total moment for Mn. The correlation length above the transition for both compositions, MnPS₃ and MnPSe₃, is illustrated in Fig. 3(b). Below the transition temperature long-range order is established with an infinite correlation length. But above the transition with increasing temperature, the correlation length decreases for both compositions. MnPSe₃ has

an uncorrelated moment at 150K, whereas the correlations persist in MnPS₃ to 300 K.

We conducted additional magnetic PDF fits for MnPS₃ above T_N over a fitting range 1.5 - 20 Å to capture the anisotropic magnetic correlations to further understand the persistence of local order. We implemented a model that distinguishes between correlation lengths in the *ab*-plane and along the *c*-axis. Our analysis reveals that the in-plane correlation (ξ_{ab}) length is approximately 15 times longer than out of plane correlation length (ξ_c) for all temperatures above T_N (see Fig. 3 (c)). This highlights that bulk MnPS₃ well approximates a 2D magnet. Undertaking the same anisotropic procedure for MnPSe₃ did not produce a clear distinction

TABLE I. Ordered magnetic moment (m), spin-angle (θ) with c -axis, and Néel temperatures of $\text{MnPS}_x\text{Se}_{3-x}$ ($x = 0, 1, 1.5, 2, 3$) at 15 K. The spin-angle for MnPS_3 was fixed to 90 degrees, as described in the text.

Samples	m (μ_B)	θ (degree)	T_N (K)
MnPS_3	4.884 ± 0.036	14.17 ± 2.091	78 Ref. [5]
MnPS_2Se	4.313 ± 0.186	20.076 ± 5.382	75.31 ± 0.63
$\text{MnPS}_{1.5}\text{Se}_{1.5}$	4.370 ± 0.132	55.260 ± 3.534	75.82 ± 1.35
MnPSSe_2	4.470 ± 0.109	58.039 ± 2.529	75.42 ± 0.65
MnPSe_3	4.666 ± 0.149	90	74 Ref. [6]

between the ab -plane and c -axis, within error. This indicates that the magnetism in MnPSe_3 is closer to three dimensional, despite the presence of a van der Waals gap between the layers.

Magnetic PDF measurements are not yet widely applied to 2D layered materials, but they can offer detailed insights. The results here show that MnPS_3 displays pronounced short-range magnetic correlations within the 2D layers well above the long range transition temperature, while this behavior is not found in MnPSe_3 . This can be observed on a qualitative level from neutron diffraction data in reciprocal space, however mPDF analysis allows for a quantitative description in real space that can be applied to various ordering length scales both above and below the Néel temperature.

B. Magnetic PDF analysis of MnPSSe_2 , $\text{MnPS}_{1.5}\text{Se}_{1.5}$, and MnPS_2Se

To gain further insight into the distinct behavior of MnPSe_3 and MnPS_3 , we conducted atomic and magnetic PDF analysis on samples with controlled S/Se content of MnPSSe_2 , $\text{MnPS}_{1.5}\text{Se}_{1.5}$, and MnPS_2Se to tune and investigate the behavior between the two materials. The same analysis procedure was applied to these samples as was used for MnPSe_3 and MnPS_3 , however the measurements were conducted on different neutron scattering instruments. Data was collected at 15, 70, 125 and 300 K. The atomic and magnetic PDF calculations for MnPSSe_2 , $\text{MnPS}_{1.5}\text{Se}_{1.5}$ were performed over the same fitting range of 1.5 - 20 Å for MnPSSe_2 and $\text{MnPS}_{1.5}\text{Se}_{1.5}$, while for MnPS_2Se , a different fitting range of 1.5 - 15 Å was selected. The variation of the fitting range on MnPS_2Se was due to a notable degradation in the quality of the fit beyond 15 Å. There could be several factors for this, such as increased stacking faults or in-plane disorder from the site mixing that lead to this behavior.

To obtain the magnetic ordering temperature of MnPSSe_2 , $\text{MnPS}_{1.5}\text{Se}_{1.5}$, and MnPS_2Se we performed neutron diffraction measurements from 25 to 125 K and obtained the integrated intensity of a magnetic reflection, as shown in Fig. 4. Fitting this to a power law shows that the ordering temperature of MnPSSe_2 , $\text{MnPS}_{1.5}\text{Se}_{1.5}$, and MnPS_2Se all occur within error around the same

temperature of 75 K (see table I), which is in between the ordering temperatures of 74 K for MnPSe_3 and 78 K for MnPS_3 .

The same iterative fitting approach was used to refine the atomic and magnetic PDF patterns as described in subsection III A. Fig. 5 shows the total PDF and isolated magnetic PDF analysis patterns for all $\text{MnPS}_x\text{Se}_{3-x}$ ($x = 0, 1, 1.5, 2, 3$) compositions at 15 K. The best fit atomic and magnetic models for MnPSSe_2 , $\text{MnPS}_{1.5}\text{Se}_{1.5}$ were obtained using the space group $R\bar{3}$ which is consistent with the space group of MnPSe_3 . Similarly, the best atomic and magnetic fits for MnPS_2Se were observed using the space group $C2/m$, which corresponds to the space group for MnPS_3 . Attempts to use alternative space groups did not produce improved fits for any compound. On comparing the mPDF patterns of all the compositions of $x = 0, 1, 1.5, 2, 3$, it is observed that the real-space magnetic intensity slowly increases with x -content, suggesting an alteration of the magnetic order. Performing the mPDF fits to the isolated magnetic data reveals a gradual increase of the spin angle with alteration of the x content in $\text{MnPS}_x\text{Se}_{3-x}$. Fig. 5(f) represents the variation of spin angle with x -content at 15 K. Table I shows the variation of calculated order moment and the spin angle of $\text{MnPS}_x\text{Se}_{3-x}$ ($x = 0, 1, 1.5, 2, 3$) at 15 K. As discussed in section III A the spin angle for MnPSe_3 was indistinguishable between 70 degrees and the previously reported value of 90 degrees, as such 90 degrees is presented here.

The results of the mPDF analysis in Fig. 5 show that a gradual change in the non-magnetic S/Se content is a parameter that can be used to directly control the magnetic spin direction. The underlying change in this process is to the crystal structure through chemical pressure as the different sized anions are altered. Fig. 5(g) shows the variation of nearest neighbor Mn-Mn and Mn-S/Se distances with x -content for $\text{MnPS}_x\text{Se}_{3-x}$ at 15 K. With progressive doping, both nearest neighbor Mn-Mn and Mn-S/Se distances decreases gradually with x -content. The decrease in the nearest neighbor Mn-Mn distance would be expected to lead to an increase in magnetic exchange interactions in the ab -plane. In addition, the change in Mn-S/Se distance will alter the crystal field environment and local anisotropy of the magnetic ion.

IV. INELASTIC NEUTRON SCATTERING

To investigate the influence of altering the non-magnetic S and Se content on the magnetic exchange interactions in the series $\text{MnPS}_x\text{Se}_{3-x}$ further we performed INS measurements on the powder samples. Measurements of the undoped compounds MnPSe_3 and MnPS_3 have been previously performed to extract the exchange interactions [8, 24], these values are shown in Table. II. Comparing the values shows that MnPS_3 has stronger in-plane interactions, however the inter-layer interactions are an order of magnitude smaller than

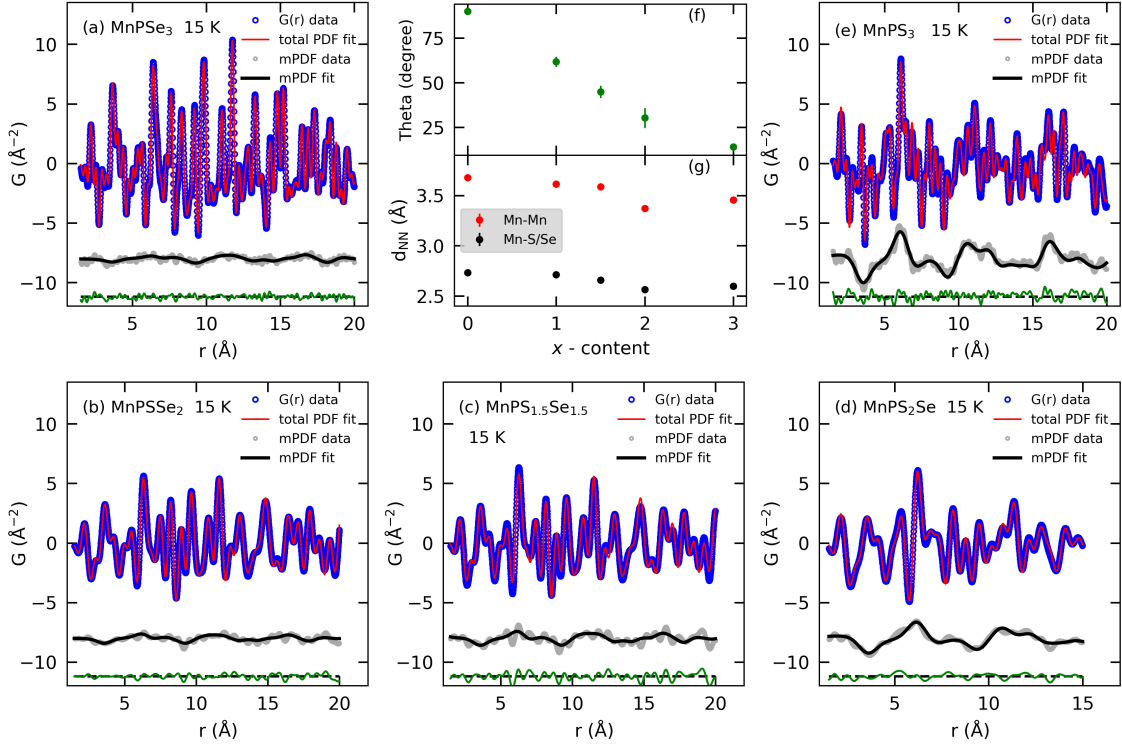


FIG. 5. Total neutron and isolated magnetic PDF patterns of (a) MnPSe_3 (b) MnPSSe_2 , (c) $\text{MnPS}_{1.5}\text{Se}_{1.5}$, (d) MnPS_2Se and (e) MnPS_3 at 15 K. The blue, red, gray, black, and green symbols represent the observed PDF data, total PDF fit, isolated magnetic PDF data, magnetic PDF fit, and overall fit residual. (f) Variation of spin angle (theta) with x -content for the series $\text{MnPS}_x\text{Se}_{3-x}$ at 15 K temperature. (g) Variation of nearest neighbor Mn-Mn and Mn-S/Se distances (d_{NN}) with x -content at 15 K for $\text{MnPS}_x\text{Se}_{3-x}$.

MnPSe_3 . This places the bulk MnPS_3 compound closer to the ideal 2D limit. This behavior was observed in the mPDF analysis reported above. In addition MnPS_3 has spin anisotropy, as evidenced by a measurable spin-gap in INS [24], which was modeled with single-ion anisotropy. No such spin-gap was observed in MnPSe_3 . Given these difference in the exchange interactions, it is somewhat surprising that MnPS_3 and MnPSe_3 order within a few degrees K of each other. The stronger (weaker) ab -plane interactions and weaker (stronger) interlayer interactions for MnPS_3 (MnPSe_3) appear to lead to a balance that results in similar ordering temperatures. How these interactions change in-between the two parent compounds is the focus of the INS measurements on $\text{MnPS}_x\text{Se}_{3-x}$ ($x = 1, 1.5, 2$).

The INS data for the full series MnPS_3 , MnPS_2Se , $\text{MnPS}_{1.5}\text{Se}_{1.5}$, MnPSSe_2 , MnPSe_3 are shown in Fig. 6. An evolution is observed in the magnetic excitation spectra as the non-magnetic S and Se ion contents are altered. MnPS_3 has the widest energy bandwidth, indicating stronger magnetic exchange interactions, and this gradually reduces as S is replaced with Se. In addition, there is an evolution in the low energy scattering, with the reported spin-gap in MnPS_3 reducing and then becoming unobservable. This is replaced with low energy scattering revealing appreciable interlayer exchange in-

teractions, as observed most strongly in MnPSe_3 .

To extract quantitative information on MnPS_2Se , $\text{MnPS}_{1.5}\text{Se}_{1.5}$ and MnPSSe_2 we follow a similar modeling process as that performed in Ref. [8]. We use linear spin wave theory with a model based on a 2D Hamiltonian on a honeycomb lattice,

$$\mathcal{H} = \sum_{i \neq j} J_{ij} \mathbf{S}_i \cdot \mathbf{S}_j = \sum_{\langle ij \rangle} 2J_{ij} \mathbf{S}_i \cdot \mathbf{S}_j$$

that included J_{1ab} , J_{2ab} and J_{3ab} intralayer exchange interactions, as well as the full spin ($S=5/2$). Note the exchange interactions have been reported to be consistent with parameters in the literature and allow comparisons between MnPSe_3 and MnPS_3 [24–27]. Alternative notation related by $J/2$ is used for MnPS_3 in Ref. [28].

The top of the band for MnPS_3 and MnPSe_3 are sharp and resolution limited for the $E_i=20$ meV measurements. There is some broadening for the MnPS_2Se , $\text{MnPS}_{1.5}\text{Se}_{1.5}$ and MnPSSe_2 . This can be attributed to a level of structural disorder introduced in the S and Se mixed compounds which would damp the excitations, as often observed in doped samples. This was accounted for in the modeling by broadening the energy resolution for the $x = 1, 1.5, 2$ analysis. A series of 1D cuts were taken at constant Q and constant E during the fitting

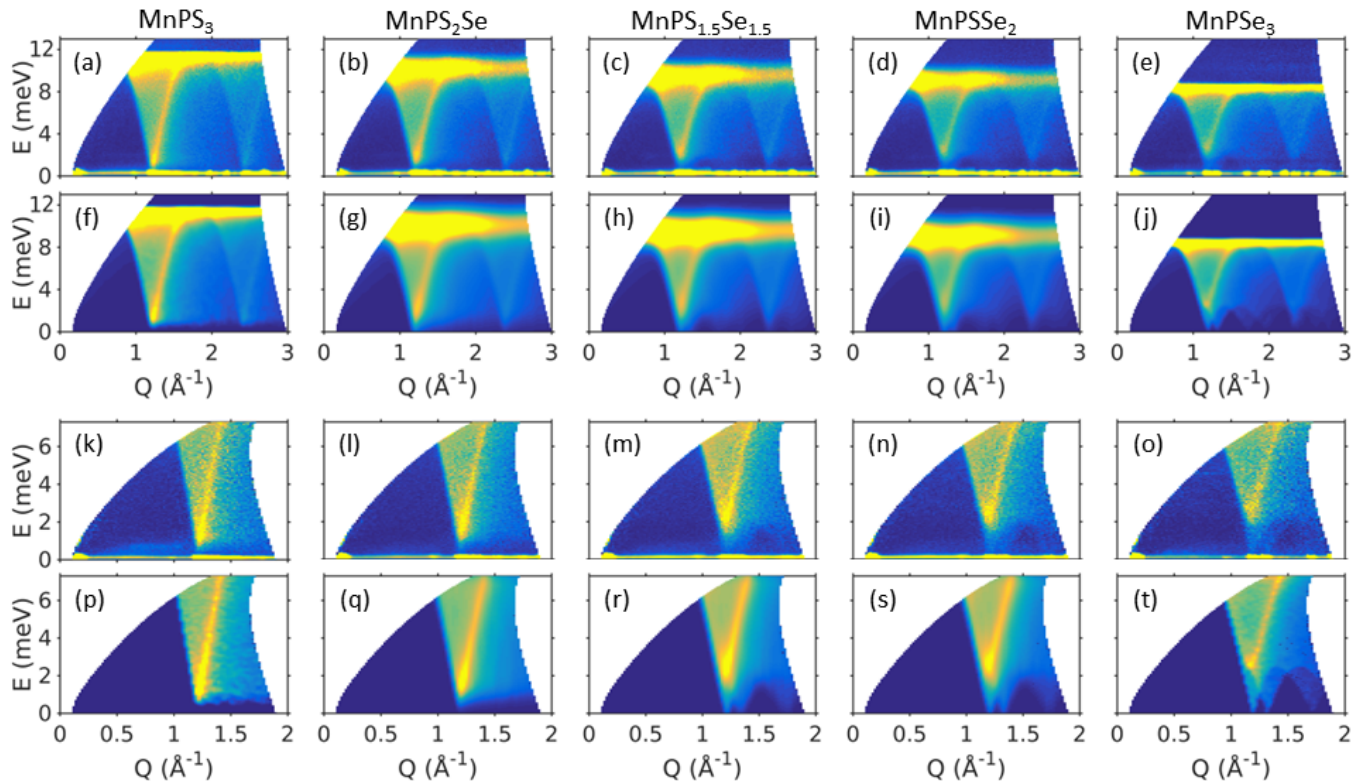


FIG. 6. Inelastic neutron scattering data and simulations for $\text{MnPS}_x\text{Se}_{3-x}$. Data collected with $E_i=20$ meV for (a) MnPS_3 , (b) MnPS_2Se , (c) $\text{MnPS}_{1.5}\text{Se}_{1.5}$, (d) MnPSSe_2 and (e) MnPSe_3 . (f)-(j) Best fit models using linear spin wave theory. Data collected with $E_i=8$ meV for (k) MnPS_3 , (l) MnPS_2Se , (m) $\text{MnPS}_{1.5}\text{Se}_{1.5}$, (n) MnPSSe_2 and (o) MnPSe_3 . (p)-(t) Best fit models using linear spin wave theory.

process. To restrict the number of variables to allow for the extraction of a minimal model the J_{1ab} , J_{2ab} and J_{3ab} interactions for MnPSe_3 and MnPS_3 were used as starting values. A scale factor was applied to model the top of the band of magnetic excitations. These values were then fixed and the interlayer interaction (J_c) and anisotropy in the form of SIA were altered in the subsequent modeling. The determined values are shown in Table. II and the comparison of experimental data and model are shown in Fig. 6.

The data and modeling shows a consistent trend of reducing the in-plane interactions and increasing the interlayer interactions as the S content is diluted with Se. This trend in exchange interactions and magnetic excitation spectra gradually altering agrees with the gradual switching of spins from in-plane (MnPSe_3) to almost fully along the c-axis in (MnPS_3) with altering S/Se content as found in the mPDF analysis.

V. CONCLUSION

In summary, the magnetic behavior of a series of 2D layered van der Waals materials $\text{MnPS}_x\text{Se}_{3-x}$ ($x = 0, 1, 1.5, 2, 3$) were investigated through atomic and magnetic

TABLE II. Exchange interactions from modeling the INS data with linear spin wave theory. All values are in meV.

	MnPS_3 Ref. [24]	MnPS_2Se	$\text{MnPS}_{1.5}\text{Se}_{1.5}$	MnPSSe_2	MnPSe_3 Ref. [8]
J_{1ab}	0.77	0.716	0.529	0.501	0.45
J_{2ab}	0.07	0.065	0.035	0.033	0.03
J_{3ab}	0.18	0.167	0.218	0.207	0.19
J_c	-0.0038	–	0.019(4)	0.025(3)	0.031
SIA	0.0086	0.0045(15)	–	–	–

PDF analysis and inelastic neutron scattering. The magnetic ordering temperature was found to remain within a few Kelvin (74 K - 78 K) for the whole series, however the spin direction, correlation length and exchange interactions evolve over a wide range as x is tuned.

The mPDF signal was isolated from the total scattering data to follow the magnetic behavior over a wide range of temperature and x composition. The mPDF results revealed short-range antiferromagnetic correlations in the paramagnetic regime. MnPS_3 was found to have a significantly longer correlation length compared to MnPSe_3 , with short range order in the 2D layers existing up to room temperature. A progressive increase in Se-

doping leads to a notable shift in spin orientation from out-of-plane to in-plane. This is found to occur gradually with x concentration.

The exchange interactions were parameterized by a minimal model antiferromagnetic Heisenberg Hamiltonian on the honeycomb lattice. These showed a gradual change in the in-plane interactions, which were largest for MnPS_3 and decreased with increasing x . Conversely the interlayer interactions are largest for MnPSe_3 and increase with x .

The change in the magnetism in $\text{MnPS}_x\text{Se}_{3-x}$ ($x = 0, 1, 1.5, 2, 3$) was induced by altering the non-magnetic S/Se ions which alters the chemical pressure, therefore structural control is central to the magnetic behavior. This highlights the ability to design and tune the magnetism in the 2D layers of $\text{MnPS}_x\text{Se}_{3-x}$ by not only controlling the x , but also through other perturbations including strain and pressure. More generally this investigation shows how the application of real space analysis of neutron data with mPDF can provide insights into 2D layered van der Waals materials where understanding local and long range ordering over a wide range of temperature of structural composition is often of inter-

est.

ACKNOWLEDGMENTS

The authors thank Benjamin Frandsen for the useful discussion. This research used resources at the High Flux Isotope Reactor and Spallation Neutron Source, a DOE Office of Science User Facility operated by the Oak Ridge National Laboratory. D.M. acknowledges support from the Gordon and Betty Moore Foundation's EPiQS Initiative, Grant GBMF9069. This manuscript has been authored by UT-Battelle, LLC under Contract No. DE-AC05-00OR22725 with the U.S. Department of Energy. The United States Government retains and the publisher, by accepting the article for publication, acknowledges that the United States Government retains a non-exclusive, paidup, irrevocable, world-wide license to publish or reproduce the published form of this manuscript, or allow others to do so, for United States Government purposes. The Department of Energy will provide public access to these results of federally sponsored research in accordance with the DOE Public Access Plan(<http://energy.gov/downloads/doepublic-access-plan>).

-
- [1] A. K. Geim and I. V. Grigorieva, *Nature* **499**, 419 (2013).
 - [2] Y. Zhang, Y.-W. Tan, H. L. Stormer, and P. Kim, *Nature* **438**, 201 (2005).
 - [3] R. Yu, W. Zhang, H.-J. Zhang, S.-C. Zhang, X. Dai, and Z. Fang, *Science* **329**, 61 (2010).
 - [4] K. S. Burch, D. Mandrus, and J.-G. Park, *Nature* **563**, 47 (2018).
 - [5] Y. Takano, N. Arai, A. Arai, Y. Takahashi, K. Takase, and K. Sekizawa, *Journal of Magnetism and Magnetic Materials* **272**, E593 (2004).
 - [6] A. Wiedenmann, J. Rossat-Mignod, A. Louisy, R. Brec, and J. Rouxel, *Solid State Communications* **40**, 1067 (1981).
 - [7] E. Ressouche, M. Loire, V. Simonet, R. Ballou, A. Stunault, and A. Wildes, *Physical Review B* **82**, 100408 (2010).
 - [8] S. Calder, A. Haglund, A. I. Kolesnikov, and D. Mandrus, *Phys. Rev. B* **103**, 024414 (2021).
 - [9] H. Han, H. Lin, W. Gan, Y. Liu, R. Xiao, L. Zhang, Y. Li, C. Zhang, and H. Li, *Applied Physics Letters* **122** (2023).
 - [10] B. Hillman, L. Norén, and D. Goossens, in *Matter and Materials Meeting* (2011) p. 50.
 - [11] X. Hou, X. Zhang, Q. Ma, X. Tang, Q. Hao, Y. Cheng, and T. Qiu, *Advanced Functional Materials* **30**, 1910171 (2020).
 - [12] X. Yan, X. Chen, and J. Qin, *Materials Research Bulletin* **46**, 235 (2011).
 - [13] C. L. Farrow, P. Juhás, J. Liu, D. Bryndin, E. S. Božin, J. Bloch, T. Proffen, and S. J. L. Billinge, *J. Phys.: Condens. Mat.* **19**, 335219 (2007).
 - [14] B. A. Frandsen, P. K. Hamilton, J. A. Christensen, E. Stubben, and S. J. L. Billinge, *Journal of Applied Crystallography* **55**, 1377 (2022).
 - [15] J. Neufeind, M. Feygenson, J. Carruth, R. Hoffmann, and K. K. Chipley, *Nucl. Instrum. Meth. B* **287**, 68 (2012).
 - [16] M. McDonnell, D. Olds, K. Page, J. Neufeind, M. Tucker, J. Bilheux, W. Zhou, and P. Peterson, *Acta Crystallogr. Sect. A* **73**, a377 (2017).
 - [17] V. O. Garlea, B. C. Chakoumakos, S. A. Moore, G. B. Taylor, T. Chae, R. G. Maples, R. A. Riedel, G. W. Lynn, and D. L. Selby, *Applied Physics A* **99**, 531 (2010).
 - [18] P. Juhás, J. N. Louwen, L. v. Eijck, E. T. Vogt, and S. J. Billinge, *Journal of Applied Crystallography* **51**, 1492 (2018).
 - [19] G. E. Granroth, A. I. Kolesnikov, T. E. Sherline, J. P. Clancy, K. A. Ross, J. P. C. Ruff, B. D. Gaulin, and S. E. Nagler, *Journal of Physics: Conference Series* **251**, 012058 (2010).
 - [20] O. Arnold, J.-C. Bilheux, J. Borreguero, A. Buts, S. I. Campbell, L. Chapon, M. Doucet, N. Draper, R. F. Leal, M. Gigg, *et al.*, *Nuclear instruments and methods in physics research section a: accelerators, spectrometers, detectors and associated equipment* **764**, 156 (2014).
 - [21] R. T. Azuah, L. R. Kneller, Y. Qiu, P. L. Tregenna-Piggott, C. M. Brown, J. R. Copley, and R. M. Dimeo, *Journal of research of the National Institute of Standards and Technology* **114**, 341 (2009).
 - [22] S. Toth and B. Lake, *Journal of Physics: Condensed Matter* **27**, 166002 (2015).
 - [23] R. Baral, J. A. Christensen, P. K. Hamilton, F. Ye, K. Chesnel, T. D. Sparks, R. Ward, J. Yan, M. A.

- McGuire, M. E. Manley, *et al.*, *Matter* **5**, 1853 (2022).
- [24] A. Wildes, B. Roessli, B. Lebech, and K. Godfrey, *Journal of Physics: Condensed Matter* **10**, 6417 (1998).
- [25] N. Sivadas, M. W. Daniels, R. H. Swendsen, S. Okamoto, and D. Xiao, *Phys. Rev. B* **91**, 235425 (2015).
- [26] J. Yang, Y. Zhou, Q. Guo, Y. Dedkov, and E. Voloshina, *RSC advances* **10**, 851 (2020).
- [27] B. L. Chittari, Y. Park, D. Lee, M. Han, A. H. MacDonald, E. Hwang, and J. Jung, *Phys. Rev. B* **94**, 184428 (2016).
- [28] D. Vaclavkova, A. Delhomme, C. Faugeras, M. Potemski, A. Bogucki, J. Suffczyński, P. Kossacki, A. R. Wildes, B. Grémaud, and A. Saúl, *2D Materials* **7**, 035030 (2020).